Analysis and forward modeling of seismic anisotropy during the ongoing eruption of the Soufrière Hills Volcano, Montserrat, 1996–2007

Diana C. Roman,[1] Martha K. Savage,[2] Richard Arnold,[3] Joan L. Latchman,[4] and Silvio De Angelis[5]

[1]   Volcanic stress field analysis has been lauded as a potentially powerful tool for midterm to long‐term eruption forecasting. However, because tectonic processes can also produce localized stress field reorientations, evidence for a direct causal link between observed stress field reorientations and magmatic activity is of critical importance. In this study, we show that local stress field reorientations preceding changes in volcanic activity at the Soufrière Hills Volcano, Montserrat, are observable using two independent measures of crustal stress (local (volcano‐tectonic) earthquake fault plane solutions and measurements of shear wave splitting in regional earthquakes). We further demonstrate that the local stress field orientation during a 6 month period preceding the onset of eruptive activity at Soufrière Hills in 1999 is highly localized and spatiotemporally variable and that the spatial pattern of precursory local stress orientations is consistent with numerically modeled patterns of stress resulting from pressurization of a vertical dike. These observations provide compelling evidence for a direct causal link between pressurization of midlevel volcanic conduit systems by ascending magma and precursory local stress field reorientations and demonstrate that seismological analysis can be used to detect subtle local changes in stress that herald eruptive activity.

1.   Introduction

[2]   Magma displaces rock as it ascends toward Earth's surface; therefore, potentially hazardous volcanoes are routinely monitored for changes in strain, including surface deformation and heightened microearthquake activity. Although this approach frequently leads to important constraints on volcano dynamics [e.g., *Umakoshi et al.*, 2001; *Elsworth et al.*, 2008], the earliest stages of precursory magmatic unrest necessarily involve subtle and/or deep changes in strain that may be too small to be detected through geodetic or microearthquake monitoring at Earth's surface, particularly when ground‐based (e.g., GPS) geodetic data are

limited and seismic monitoring networks are sparse. Thus, traditional strain field monitoring approaches are limited in their ability to provide accurate early warnings of impending eruptive activity. Direct monitoring of precursory changes in stress, rather than strain, has been heralded as a promising approach to overcoming this limitation, and observed precursory changes in the local stress field orientation beneath restless volcanoes have been hypothetically linked to pressurization of the midlevel magmatic conduit system [e.g., *Umakoshi et al.*, 2001; *Gerst and Savage*, 2004; *Roman et al.*, 2004]. However, the application of stress field analysis in volcano monitoring has been hindered by an incomplete understanding of the stress field reorientation mechanism and a lack of strong evidence for a direct causal link between the observed stress field changes and magmatic activity.

[3]   A growing number of studies of temporal changes in volcano‐tectonic (VT) earthquake fault plane solution (FPS) orientations [e.g., *Umakoshi et al.*, 2001; *Roman et al.*, 2004; *Roman et al.*, 2006; *Lehto et al.*, 2010] and regional split shear (S) wavelet polarizations [e.g., *Gerst and Savage*, 2004; *Bianco et al.*, 2006; *Savage et al.*, 2010b] have documented ephemeral ~90° reorientations of the axis of maximum compression (σ_1) in the vicinity of restless volcanoes during the weeks to months preceding eruptive

[1]Department of Geology, University of South Florida, Tampa, Florida, USA.
[2]School of Geography, Environment and Earth Sciences, Victoria University of Wellington, Wellington, New Zealand.
[3]School of Mathematics, Statistics, and Operations Research, Victoria University of Wellington, Wellington, New Zealand.
[4]Seismic Research Centre, University of the West Indies, St. Augustine, Trinidad and Tobago.
[5]Montserrat Volcano Observatory, British Geological Survey, Flemings, Montserrat.

activity, which may be linked to preeruptive pressurization of the midlevel volcanic conduit system. Specifically, the orientations of VT FPS P axes and fast polarizations of split S wavelets (Φ), both of which may be taken as proxies for the orientation of σ_1, have been observed to change by ~90° preceding eruptions. However, while multiple authors have hypothesized inflation of a dike trending parallel to (and opening perpendicular to) regional σ_1 as the cause of the ~90° reorientation [e.g., *Gerst and Savage*, 2004; *Roman et al.*, 2006], and several studies have shown that numerical models of dike inflation produce stress changes of sufficient magnitude and orientation to cause the observed reorientations [*Gerst and Savage*, 2004; *Roman*, 2005], other possible causes have not been ruled out, and conclusive evidence for the dike inflation model has not been presented. Alternative mechanisms for real changes in crustal stress field orientations include regional- or arc-scale tectonic processes [e.g., *Beroza and Zoback*, 1993; *Tadokoro and Ando*, 2002], although it is not clear whether such processes could rotate the regional stress field by ~90° on relatively short timescales. Apparent ~90° changes in Φ may also result from systematic temporal variations in earthquake locations or frequency contents, or through microscale fluid movement between microcracks in rock (i.e., in analytical models of anisotropic poroelasticity (APE), shear waves polarized at right angles to maximum horizontal compression are faster than shear waves parallel to maximum horizontal compression under conditions of high pore fluid pressures [*Zatsepin and Crampin*, 1997, equation 5.38 and Figure 9]). To differentiate between the above mechanisms, it is necessary to determine (1) whether the change in stress field orientation is truly localized (i.e., on the scale of kilometers) to the region beneath the volcano and (2) whether the local stress field reorientation has a spatial pattern consistent with that predicted by generalized numerical models of maximum horizontal stresses resulting from dike inflation [e.g., *Bonafede and Danesi*, 1997]. Furthermore, observation of contemporaneous changes in both VT FPS orientations and Φ at a single volcano would confirm that the stress field change is real and validate the use of either technique for real-time volcanic stress field monitoring.

[4] In this study, we test the hypothesized dike inflation mechanism for local stress field reorientation preceding volcanic activity by calculating, analyzing, and forward modeling split S wavelet polarizations on the island of Montserrat, and on the neighboring islands of St. Kitts and Antigua, during a period of cyclic activity at the Soufrière Hills Volcano, Montserrat. The 1995 to present Soufrière Hills eruption typifies many other long-term andesitic-dacitic dome-building eruptions, such as those at Mount Unzen, Japan (1990–1995) [e.g., *Nakada et al.*, 1999]; Mount St. Helens, Washington (1980–1986 and 2004–2006) [e.g., *Lipman and Mullineaux*, 1981; *Sherrod et al.*, 2008]; Galeras, Colombia (1988 to present) [e.g., *Cortés and Raigosa*, 1997]; Santiaguito, Guatemala (1922 to present) [e.g., *Bluth and Rose*, 2004]; and Guagua Pichincha, Ecuador (1999–2001) [e.g., *Garcia-Aristizabal et al.*, 2007] and. to date, has comprised four discrete phases of extrusive activity each separated by up to 2 years of residual to no lava extrusion [e.g., *Elsworth et al.*, 2008]. Soufrière Hills has been monitored continuously by a network of broadband

seismometers since 1996 [*Luckett et al.*, 2007], and an earlier study of FPS for VT earthquakes recorded beneath Soufrière Hills between 1996 and 2007 documented ~90° changes in local FPS P axis orientations (a weak proxy for σ_1) weeks to months before each new phase of activity [*Roman et al.*, 2006]. The longevity and periodic nature of this major, well-monitored eruption, along with prior work documenting the occurrence of precursory stress field changes, provide a unique opportunity to test and refine theoretical models and practical approaches for volcanic stress field monitoring.

2. Background

2.1. Setting and Activity of the Soufrière Hills Volcano

[5] The Soufrière Hills Volcano occupies the southern third of the island of Montserrat, in the northern segment of the Lesser Antilles island arc (Figure 1). Soufrière Hills has been the center of active volcanism on Montserrat since at least 170 Ka [*Harford et al.*, 2002]. Additional details on the setting of the Soufrière Hills Volcano are given by *Kokelaar* [2002].

[6] As of 2010, the current eruption of the Soufrière Hills Volcano has been ongoing for 15 years and has so far consisted of four discrete phases of extrusive activity. The eruption began in mid-1995 following approximately 3 years of escalating seismic activity, with a series of VT earthquake swarms beginning in January 1992 that intensified in 1994 [*Ambeh and Lynch*, 1996]. A phreatic explosion on 18 July 1995 marked the onset of the phreatic phase of the eruption, which continued until the first emergence of lava at the volcano's summit in September 1995 [e.g., *Gardner and White*, 2002]. Soufrière Hills then remained in continuous eruption until March 1998. During this first phase of activity, a transition from effusive (dome building) to explosive volcanism occurred in June–August 1997 with the onset of a well-documented series of Vulcanian explosions that continued through October 1997. The second phase of the eruption began in November 1999, following a pause in the eruption of approximately 20 months. The second phase of the eruption lasted until July 2003 and was characterized by dome growth punctuated by episodes of dome collapse and explosions, including a major dome collapse in July 2003. Eruptive activity paused a second time beginning in August 2003, resuming approximately 2 years later with the onset of the third phase of lava extrusion in August 2005. Dome growth during this third phase was initially sluggish, with extrusion rates increasing significantly in February–March 2006, followed by significant explosions in May 2006 and January 2007, and a major dome collapse on 20 May 2006. Phase three of the eruption ended in April 2007. Following a third major pause in dome growth, residual explosive activity continued until mid-2008, when the fourth phase of lava extrusion began (for details, see "A Chronology of the Current Eruption," available from the Montserrat Volcano Observatory (http://www.mvo.ms or http://www.mvo.ms/en/soufriere-hills-volcano/history-of-the-volcano/chronology-of-current-eruption/chronology-of-current-eruption)).

2.2. Seismic Monitoring on Montserrat

[7] A dense network of seismometers has operated nearly continuously on Montserrat since 1995, with a configuration
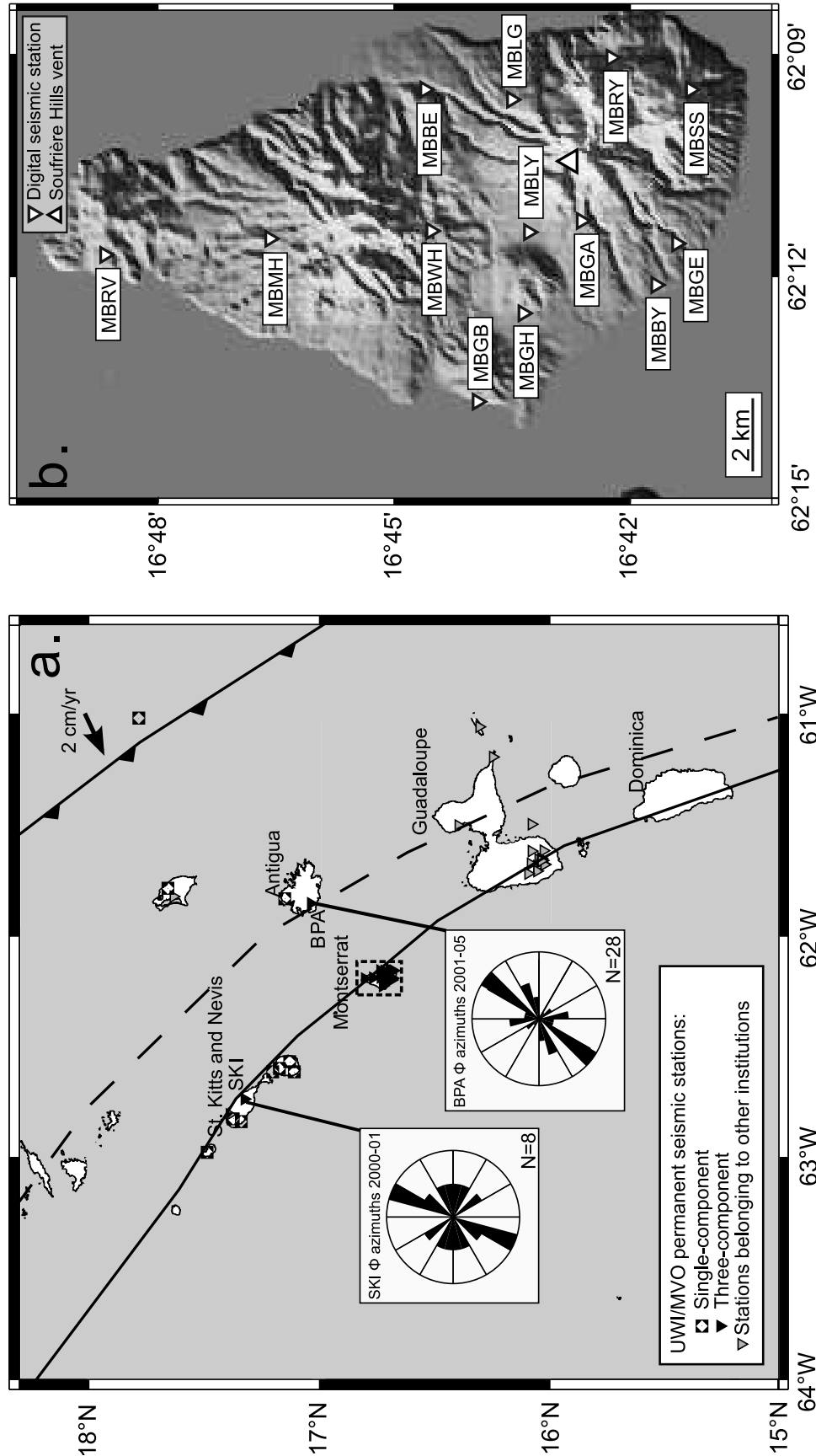
Figure 1. (a) Regional map showing the location of Montserrat (dashed box) relative to other Caribbean islands, locations of TRN seismic stations operated by the University of the West Indies Seismic Research Centre, and rose diagrams of Φ for two three-component stations (SKI and BPA) located on St. Kitts and Antigua, respectively. The toothed line indicates the surface trace of the subduction zone, the dashed line indicates the trend of the outer (older) arc, and the solid line indicates the trend of the inner (modern) arc (all after *Bouysse and Westercamp* [1990]). The plate convergence vector is from *DeMets et al.* [2000]. (b) Map of Montserrat showing names and locations of all digital seismic stations (inverted triangles) operated by the Montserrat Volcano Observatory between October 1996 and September 2007 (note that not all stations are three component and not all stations operated from 1996 to 2007; see *Roman et al.* [2008] for dates of individual station operation). White triangle marks the approximate location of the Soufrière Hills vent.

that has changed several times during the eruption. Beginning in July 1995, the Montserrat seismic monitoring system included a telemetered network of short-period, primarily vertical component, analog 1 Hz seismometers [e.g., *Luckett et al.*, 2007]. This network was replaced in October 1996 by a telemetered digital seismic network (Figure 1b). Initially, the digital network included five Guralp CMG-40T broadband seismometers and three Integra LA100 1 Hz vertical seismometers [e.g., *Luckett et al.*, 2007]. In time, additional broadband stations were added to the network. Several of the stations in operation between July 1995 and present were destroyed by activity at the volcano. The current (2010) incarnation of the seismic monitoring system dates from September 2004 and reflects the addition, relocation, and replacement of many stations. By March 2005, most stations included a CMG-40T sensor. Locations and all available information on the dates of operation for the analog and digital stations through 2007 are given by *Roman et al.* [2008].

2.3. Regional Seismic Monitoring, Tectonics, and Seismicity

[8] During the study period, the principal regional seismic monitoring network in the Lesser Antilles consisted of over 50 permanent seismic stations located in the English-speaking islands and run by the Seismic Research Centre (SRC) at The University of the West Indies (the TRN network, Figure 1a). Most TRN stations have 1 Hz Mark Products L4-C vertical analog sensors, but several TRN stations have 1 Hz Lennartz LE-3D three-component seismometers, Guralp CMG5 3-component accelerometers, or Guralp CMG-40T three-component broadband seismometers. Signals from each sensor are digitized at 100 samples/second, and analyzed by an automated triggering algorithm for possible seismic events [*Beckles et al.*, 1992]. Triggered signals are then screened and genuine earthquakes are processed by SRC analysts using the analysis package Wurstmachine [*Beckles et al.*, 1977].

[9] The Lesser Antilles island arc arose from subduction of the North American plate beneath the Caribbean plate. The plates converge with a northeast-southwest orientation, at a rate of approximately 2 cm/yr [e.g., *Stein et al.*, 1988] generating the significant seismic and volcanic activity characteristic of the region. Depths of regional earthquakes increase westward, and shallow (<10 km depth) and intermediate (10–50 km depth) earthquakes are located predominantly east of the volcanic arc [e.g., *Stein et al.*, 1982; *McCann and Pennington*, 1990]. FPS for regional earthquakes in the vicinity of Montserrat typically have thrust mechanisms consistent with subduction processes [e.g., *Stein et al.*, 1982; *Roman et al.*, 2008]. Their P axes are generally oriented arc normal, indicating that maximum regional compression along the northernmost segment of the Lesser Antilles arc is arc normal, or NE-SW in the vicinity of Montserrat. This orientation is consistent with the findings of *Bonneton and Scheidegger* [1981], who measured joint orientations on Montserrat and neighboring islands and calculated a principal stress orientation (σ_1) for Montserrat of 32° (all orientations are given as azimuths clockwise from north). *Wadge* [1986] mapped the orientation of dikes in the Lesser Antilles and found a predominant NE-SW orientation for dikes in the vicinity of Montserrat, again indicating that the regional stress field in this segment of the Lesser Antilles arc is characterized by NE-SW maximum compression.

3. Methods

3.1. Shear Wave Splitting Analysis

[10] We analyzed shear wave splitting (SWS) in regional earthquake waveforms from all three-component stations on Montserrat and neighboring islands (TRN stations within 100 km of Montserrat) whose orientations could be verified through analysis of Rayleigh wave particle motions (i.e., by comparison of the Rayleigh wave particle motion to the event-station back azimuth) and (for Montserrat stations) which operated continuously throughout the entire study period (October 1996 to September 2007). The latter criterion permitted us to examine changes through time on individual Montserrat stations, avoiding potential issues of location-dependent seismic anisotropy [*Savage et al.*, 1989]. On Montserrat broadband stations MBBY, MBGB, MBGH, and MBRY, we analyzed all events recorded between October 1996 and September 2007 that had been classified by Montserrat Volcano Observatory analysts as "regional" according to a standard classification scheme [*Miller et al.*, 1998]. For TRN stations SKI and BPA, located on St. Kitts and Antigua, respectively, we analyzed all regional (S-P intervals > 10 s) and local earthquakes recorded between October 1996 and September 2007 that were cataloged by SRC analysts during routine data processing. Unfortunately, the number of earthquakes available for analysis on TRN stations was severely limited due to frequent station outages during the study period: SKI was operational only between 2000 and 2001, and BPA was operational only between 2001 and 2005. We analyze tectonic, rather than volcanic (VT), earthquakes to allow a comparative analysis of SWS between Montserrat (where VT earthquakes are frequent) and St. Kitts and Antigua (which have minimal VT seismicity), and because the rate of VT earthquakes fluctuated significantly during our study period (with some periods of the Soufrière Hills eruption having little to no VT seismicity [*Roman et al.*, 2008]).

[11] For SWS analysis, we employ a semiautomated method [*Wessel*, 2008] based on the Shear wave Birefringence Analysis (SHEBA)/Silver and Chan algorithms [*Teanby et al.*, 2004; *Silver and Chan*, 1991], which analyzes multiple time windows around a manual S wave time pick (all S wave arrival times were repicked for this study) and performs cluster analysis to determine and automatically grade the best estimate of Φ and delay time (*dt*). The *Wessel* [2008] method first applies a set of user-defined filters (Table 1) to the earthquake waveform to find the three frequency bands with the highest signal-to-noise ratios. Each waveform is then analyzed three times (once for each of the three best filters), and may contribute up to three splitting measurements: Measurements from waveforms in which anisotropy is frequency dependent are therefore downweighted in subsequent analyses of the results. Because low seismic velocities near the Earth's surface are assumed to result in near-vertical raypath arrivals, particularly on volcanic islands, we do not apply a strict "shear wave window" criterion [e.g., *Booth and Crampin*, 1985] to the data, as this practice is believed to unnecessarily elimi-

**Table 1.** Filters Applied to Waveforms Prior to SWS Analysis

Filter	Low Frequency (Hz)	High Frequency (Hz)
1	0.2	5
2	0.2	8
3	0.4	6
4	0.4	9
5	0.4	12
6	0.6	7
7	0.6	10
8	1	12
9	1	5
10	1	8
11	2	9
12	2	12
13	3	8
14	4	12

nate too many events from the analysis [*Savage et al.*, 2010b]: For example, the critical angle of a near-horizontal (10°) seismic wave intersecting the boundary between the two topmost layers in a velocity model developed for Montserrat by *Paulatto et al.* [2010] is ~30° from vertical, well within the shear wave window. Instead, we rely on a strict two-level grading scheme to evaluate the results of SWS analysis: Automated assignment of an A, B, C, or D grade is based on the clustering properties of the solutions found using a set of slightly different analysis windows around the user-specified S wave pick [*Savage et al.*, 2010a, 2010b]. Specifically, the code compares all identified clusters of solutions and assigns a grade based on the uniqueness of the best cluster solution. If there is a secondary cluster that has more than half the number of measurements in the "best" cluster, and also has low variance and a significantly different solution from the best one, the solution is given a grade of C or D; Cluster grade B is given if any secondary clusters with significantly different solutions have between five measurements and half the measurements in the best cluster, and A is given otherwise (for details, see *Savage et al.* [2010a]). The automated grading scheme also marks measurements with ambiguous "NULL" polarizations (these were discarded). Measurements which received an A or B grade in automated grading were then manually evaluated and assigned a second A–D grade based on stability and average error of the solutions over different time windows, evidence of cycle skipping, similarity between the two rotated and transformed S wavelets, and
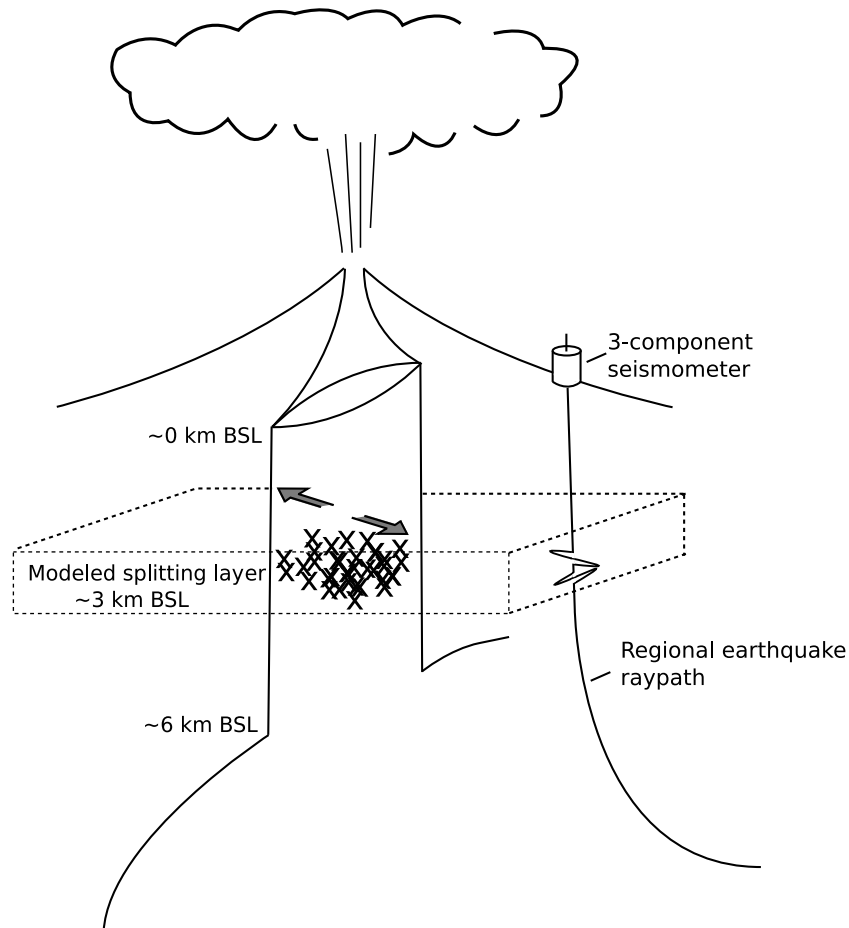
Figure 2. Schematic illustration of the model configuration, showing the depth extent of the model dike, depth of the modeled splitting layer, which corresponds to the approximate depth range of volcano-tectonic (VT) earthquakes with ~90° rotated fault plane solution (FPS) (represented by crosses) recorded during the 1995 to present eruption [e.g., *Roman et al.*, 2008].
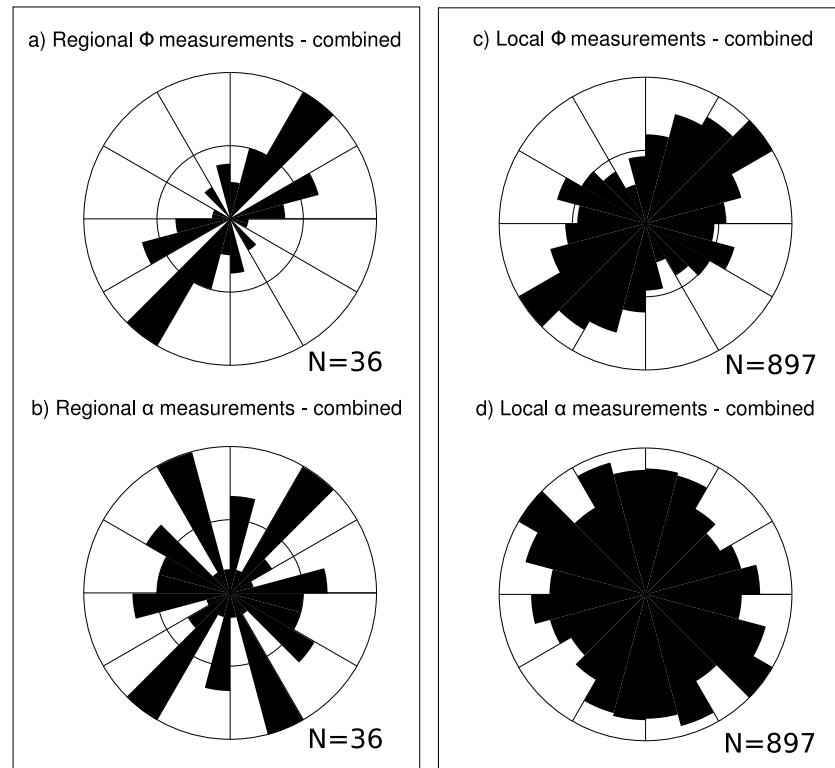
Figure 3. Rose diagrams of combined results (all stations, entire study period) showing (a) final (split) polarizations, Φ, and (b) initial polarizations, α, for all measurements on TRN network stations SKI and BPA, (c) final (split) polarizations, Φ, and (d) initial polarizations, α, for all measurements on Montserrat stations MBBY, MBGB, MBGH, and MBRY. N indicates the number of measurements in each rose diagram.

linearity of the resolved (unsplit) S wave particle motion [e.g, *Gerst and Savage*, 2004]. In this study, we present and analyze only the SWS measurements assigned an A or B grade in both automated and manual grading (see the auxiliary material for examples of A–D graded events).[1]

3.2. Stress Field Modeling

[12] Modeled Φ orientations (Φ_M) were calculated with Coulomb 3.1 [*Toda et al.*, 2005; *Lin and Stein*, 2004] using standard elastic moduli appropriate for the Earth's crust (shear modulus of 32 GPa, Poisson's ratio of 0.25, and an effective coefficient of internal friction of 0.4 [e.g., *Toda et al.*, 2005]). Coulomb 3.1 is a finite difference code that allows calculation in an elastic half-space of static displacements, stresses, and strains resulting from fault slip or inflation/deflation of simple magmatic sources (e.g., opening tensile cracks, or dikes, may be modeled using an Okada dislocation [*Okada*, 1992]). To limit the number of model free parameters, we assumed an isotropic regional stress field, and limited the width/length range of the modeled dikes to values consistent with field observations of eroded dikes on neighboring islands [*Wadge*, 1986]. We also neglected topography. These two assumptions are not strictly

valid since as we point out below, exposed dikes align in the regional stress direction. However, topography is very difficult to model, and other studies have found that to explain time variations in stress, relatively isotropic fields are needed [e.g., *Gerst and Savage*, 2004; *Savage et al.*, 2010b]. Because SWS analysis only gives information on stresses normal to the raypath (assumed to be vertical during the final stages of propagation), we evaluate the models in a horizontal 2-D slice at the midpoint of the modeled dike (e.g., Figure 2). Modeled dikes extend from 0 to 6 km below sea level (BSL) consistent with the apparent depth range of the Soufriere Hills conduit to the topmost magma chamber as indicated by petrologic observations [e.g., *Murphy et al.*, 2000]. Φ_M orientations at 3 km BSL are used for comparison to Φ measurements, to test the hypothesis that strong changes in local stresses inferred from FPS for VT earthquakes (located at approximately ~3 km BSL) are also recorded by split S wavelets (e.g., Figure 2). In this case, the maximum principal stress in the vicinity of the dike (σ_{1L}) is horizontal and may be taken as Φ_M. In total, 108 models were calculated: A constant dike width (inflation)-to-length ratio of 1/1000 was assumed, and dike widths (in 0.5 m increments) from 0.5 to 3.0 m were tested. Tested dike azimuths ranged from 0 to 170°, in 10° increments (we tested all possible dike orientations due to a controversy concerning the orientation of the Soufriere Hills conduit, and accompanying uncertainty about the orientation of the "background" stress field beneath Montserrat; see Discus-

---

[1]Auxiliary materials are available in the HTML. doi:10.1029/2010JB007667.
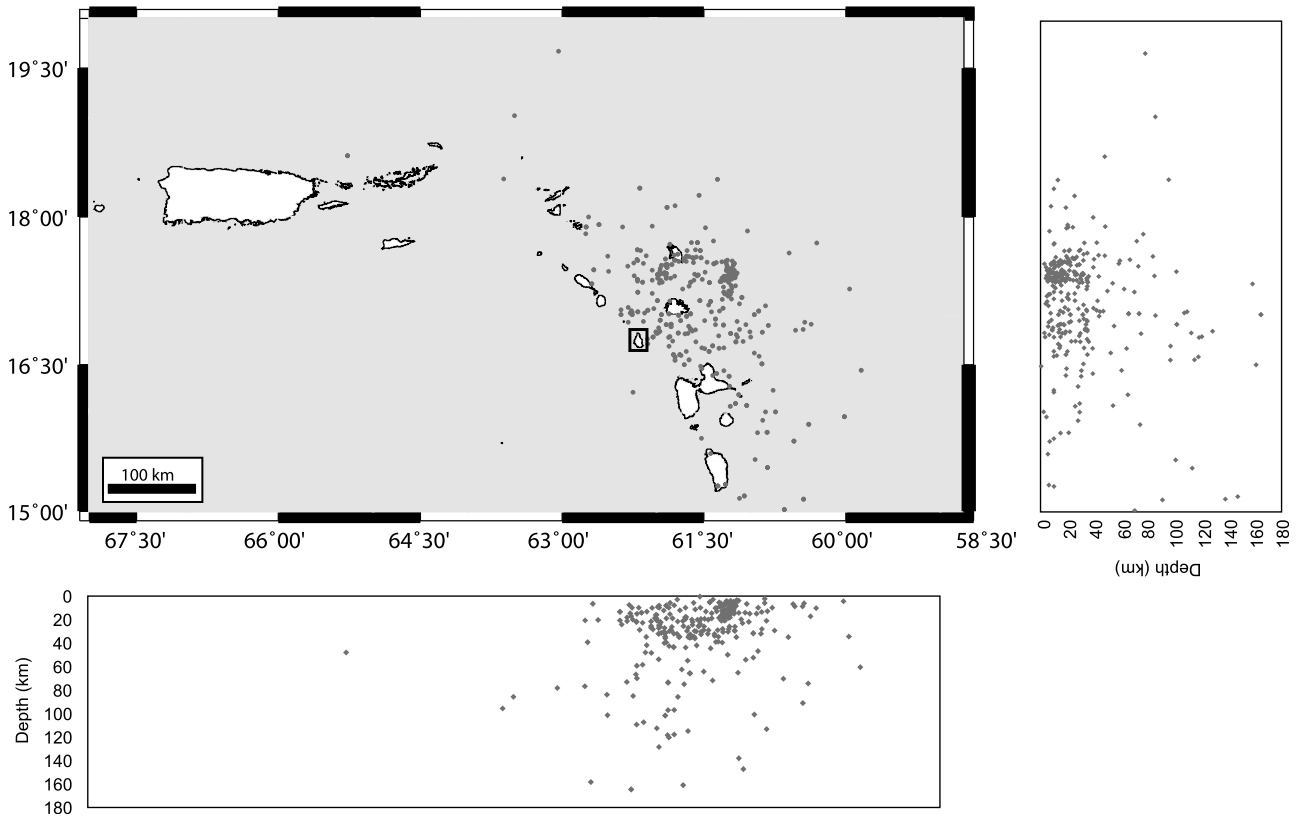
Figure 4. Map and cross sections showing the locations of earthquakes corresponding to A/B quality SWS measurements. The location of Montserrat is indicated by the black box.
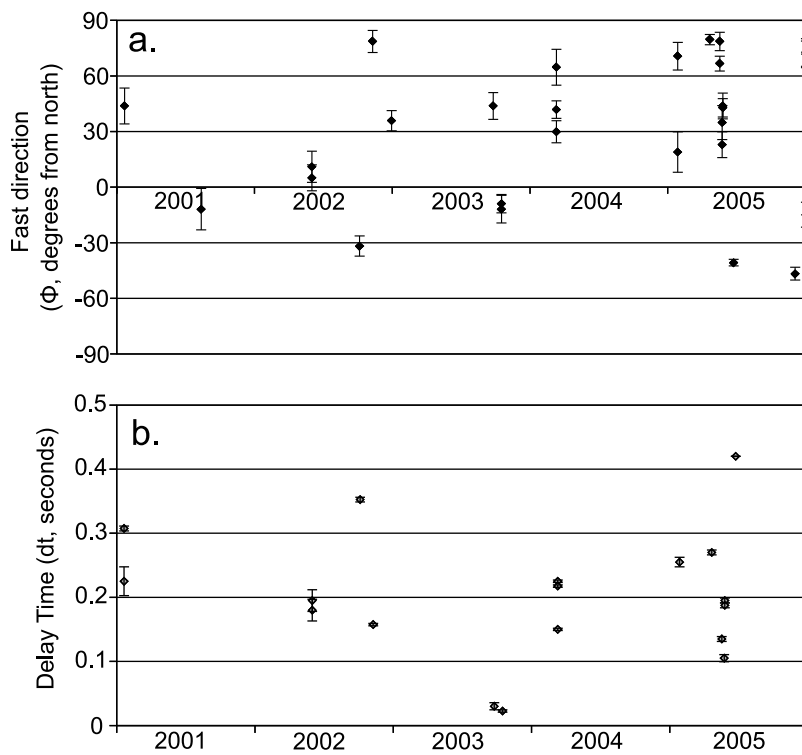
Figure 5. Individual measurements of (a) Φ and (b) *dt* on Antigua station BPA through time, including 95% confidence intervals (vertical bars).
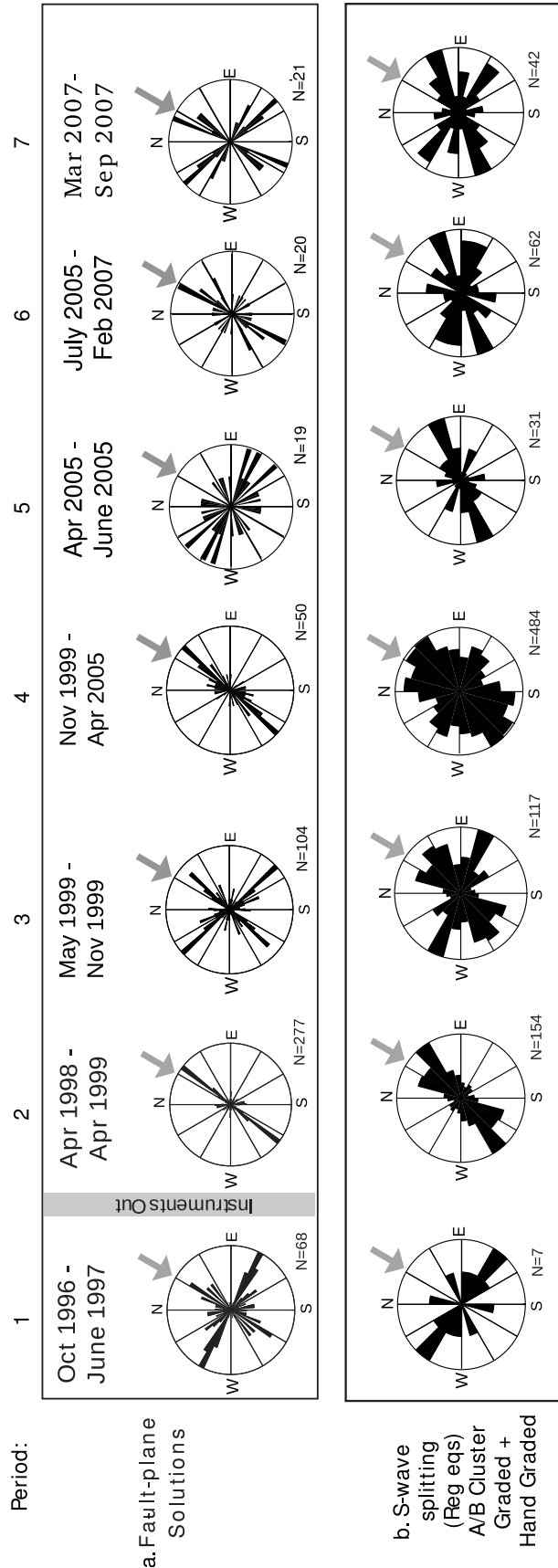
Figure 6. (a) Comparison of VT earthquake FPS P axis azimuths [from *Roman et al.*, 2006, 2008]) to (b) combined A/B-quality measurements of Φ in regional earthquakes from equivalent periods. N indicates the number of measurements in each rose diagram. Gray arrows indicate the approximate azimuth of regional maximum compression inferred from dike orientations and Φ on neighboring islands (see text for details).

Table 2. Mean Directions (θ) and Concentration Parameters ($\hat{\kappa}$)[a]

Period	Data	n	θ	95% MOE	$\hat{\kappa}$	95% MOE
2	P axis	277	30.5	7.4	0.66	0.18
2	Φ	154	45.3	7.7	0.87	0.25
4	P axis	50	34.2	8.5	1.47	0.55
4	Φ	484	44.3	12.9	0.28	0.13
6	P axis	20	34.6	24.3	0.76	0.69
6	Φ	62	88.4	21.1	0.48	0.37

[a]With 95% confidence margins of error (MOE), estimated from fitted Von Mises distributions for period 2, 4, and 6 data.

sion). The best fit model was chosen as that which minimized model misfit, defined as

$$\frac{\sum (\Phi_M - \Phi)}{n} \qquad (1)$$

where Φ_M is the modeled maximum horizontal stress orientation beneath a given station in degrees, Φ is the dominant orientation of measured Φ at a given station (or in cases where Φ is bimodal, the orientation of the ephemeral Φ trend) in degrees, and n is the number of stations at which observations were obtained. Because we assumed that the splitting occurred along the shallow, vertical component of the ray, in the same shallow depth range as the VT earthquakes with rotated FPS (i.e., 1–3 km BSL [*Roman et al.*, 2008]), we examine the orientation of Φ directly beneath the station (e.g., Figure 2).

4. Results, Statistical Analysis, and Stress Field Modeling

[13] SWS analysis resulted in 897 A/B-quality measurements on four Montserrat seismic stations, and 36 A/B-quality measurements on two TRN seismic stations (Figure 3). Measurements from TRN stations show a dominant NE-SW Φ orientation (Figure 3a), while measurements from Montserrat stations show a dominant NE-SW Φ orientation and a secondary NW-SE Φ orientation (Figure 3c). Initial polarizations (α) for earthquakes recorded on TRN stations (Figure 3b) appear to be randomly distributed. However, a weak NW-SE trend apparent in α for earthquakes recorded on Montserrat stations (Figure 3d) is approximately parallel to Φ measurements from analysis of SKS/SKKS splitting on Montserrat stations by *Piñero-Feliciangeli and Kendall* [2008], suggesting a deeper layer of anisotropy beneath Montserrat characterized by a NW-SE polarization and possibly related to mantle flow. Earthquakes corresponding to A/B-quality splitting measurements are located throughout northern Lesser Antilles, but are concentrated near Montserrat and located mostly in the overriding plate (<40 km BSL). Some earthquakes appear to be located in the subducting slab, with depths down to ~160 km BSL (Figure 4).

4.1. Spatiotemporal Analysis of Results

[14] Measurements of SWS provide evidence for localized temporal variations in Φ consistent with a volcanically induced change in the local stress field orientation beneath Montserrat during the study period. For the two off-island stations SKI and BPA, measurements of Φ are oriented

predominantly NE-SW, or arc normal (Figure 1a), and there is no indication of a temporal change in Φ or dt beneath Antigua during the study period (Figure 5). In contrast, combined measurements of Φ from Montserrat seismic stations show a more complex temporal pattern: Figure 6b shows combined measurements of Φ from Montserrat stations plotted for the seven time periods of variable local stress field orientation defined by *Roman et al.* [2008] on the basis of VT FPS orientations, and indicates that Φ varies contemporaneously with previously observed changes in VT FPS P axis orientations through early 2005 (periods 1–4 in Figure 6). From 2005 on, the orientation of local stress becomes less clear in both the FPS and SWS data sets and is poorly correlated (periods 5–7 in Figure 6). The agreement between the two data sets is most apparent between April 1998 and April 2005 (periods 2–4 in Figure 6), when a local reorientation of both Φ and P axis orientation occurred during the 6 months preceding the renewal of extrusive activity in November 1999 (period 3 in Figure 6). However, measurements of Φ during periods 3 and 4 show a higher degree of heterogeneity than corresponding P axis orientations, suggesting additional spatial and/or temporal changes in local stress between 1999 and 2005.

4.1.1. Statistical Analysis of FPS P Axis Orientations and Combined Measurements of Φ

[15] A statistical analysis was performed to test the robustness of the apparent agreement between trends in P axis orientations and Φ, stability in P axis orientation and Φ during quiescent periods (periods 2, 4 and 6 in Figure 6), and high degree of heterogeneity in Φ compared to P axis orientations (periods 1, 3, 5, and 7 in Figure 6). The axial Von Mises distribution [*Mardia and Jupp*, 2000]

$$f_a(\theta, \mu, \kappa) = \frac{1}{2\pi I_o(\kappa)} e^{\kappa \cos(2(\theta - \mu))} \; (0 \leq \theta < \pi) \qquad (2)$$

is used as the basis for parameter estimation and hypothesis testing, and parameter estimation (μ, κ) is done by maximum likelihood. Parameter estimates for the quiescent periods 2, 4 and 6, with simple distributions of P axes and Φ, are shown in Table 2.

[16] We first address the consistency of the two methods of stress analysis using the Watson-Williams test [*Watson and Williams*, 1956]. This parametric test assumes that
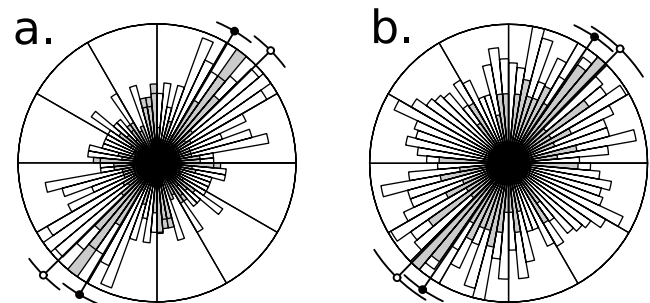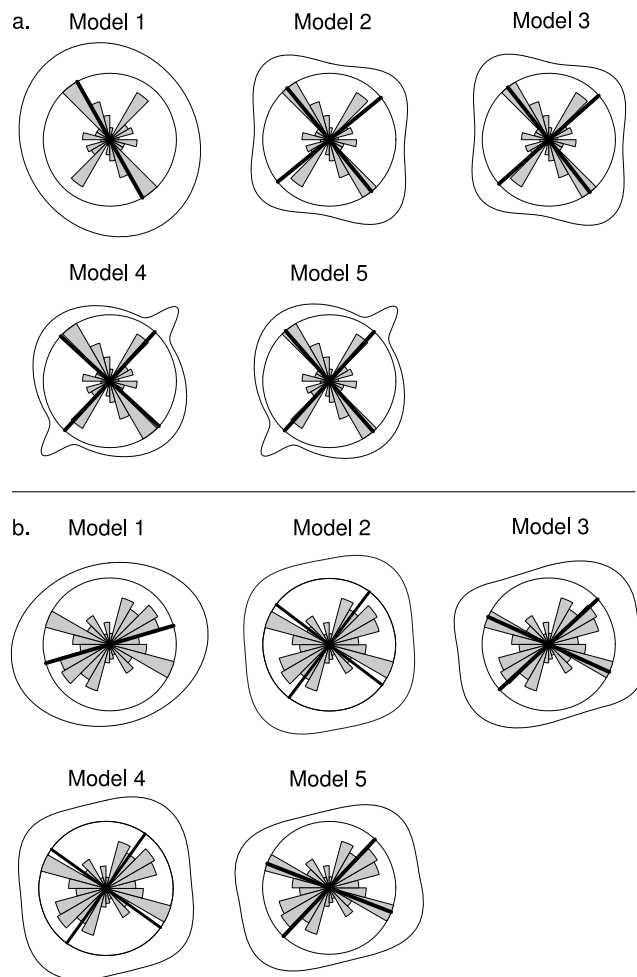

Figure 7. Distributions of orientations in (a) period 2 and (b) period 4. Dark bars are the P axis data; white bars are the Φ data. Confidence intervals for the fitted mean orientation are shown as small arcs.

Table 3. Estimated Parameters of Fitted Models to Stress Data[a]

Model	p_1	p_2	μ_1	μ_2	κ_1	κ_2	AIC	Npar
			FPS					
1	1.0000		150.6		0.23		383.6	2
2	0.5876	0.4124	140.8	50.8	1.84	1.84	369.3	3
3	0.5877	0.4123	141.9	48.5	1.85	1.85	370.9	4
4	0.8083	0.1917	132.5	42.5	0.74	27.06	364.1	4
5	0.8075	0.1925	139.0	42.2	0.76	27.03	364.9	5
			SWS					
1	1.0000		73.6		0.43		423.4	2
2	0.5665	0.4335	37.2	127.2	1.09	1.09	431.9	3
3	0.5298	0.4702	43.3	111.3	1.37	1.37	421.9	4
4	0.6298	0.3702	35.6	125.6	0.93	1.42	433.8	4
5	0.6876	0.3125	47.4	114.4	0.94	2.37	423.6	5

[a]With AIC values and numbers of free parameters (Npar).

two data sets are well represented by Von Mises distributions with a common concentration parameter, κ, and tests for a difference in mean directions. Using a version of the test appropriate for axial distributions we find a small, but statistically significant, difference of 14.9° (±11°, $p = 0.0111$) between FPS P axes and Φ in period 2 This confirms that the P axis and Φ orientations are similar in period 2. Like period 2, period 4 is characterized by a relatively simple distribution of FPS P axes but has a more heterogeneous distribution of Φ, as indicated by the large concentration κ for FPS and small κ for Φ (Table 2). With such different concentration parameters, the Watson-Williams test is not appropriate for period 4 data, but a simple significance test using the standard errors from the estimates in Table 2 finds no statistically significant differences between the two directions ($p = 0.2042$) yields a standardized difference of z = −1.27 and a p value of 0.2042, suggesting a common direction. Mean directions and confidence intervals for period 2 and 4 data are illustrated in Figure 7.

[17] Watson-Williams tests may also be used to test the stability of orientations between periods (i.e., whether the orientation during quiescent periods is consistent before and after an ephemeral reorientation). Between periods 2 and 4 we find no evidence for a difference between the mean angles of FPS P axes ($p = 0.6095$), nor Φ ($p = 0.8930$), confirming that the orientations are stable between these periods. However, while a test for a difference in P axis orientations between periods 4 and 6 indicates stability ($p = 0.7764$), the difference in Φ between periods 4 and 6 is statistically significant ($p = 0.0001$), confirming the apparent scatter and decorrelation of the SWS measurements beginning in June 2005.

[18] Finally, we test the hypothesis that both P axis and Φ measurements preserve a bimodal distribution with modes at right angles during period 3 (consistent with the dike
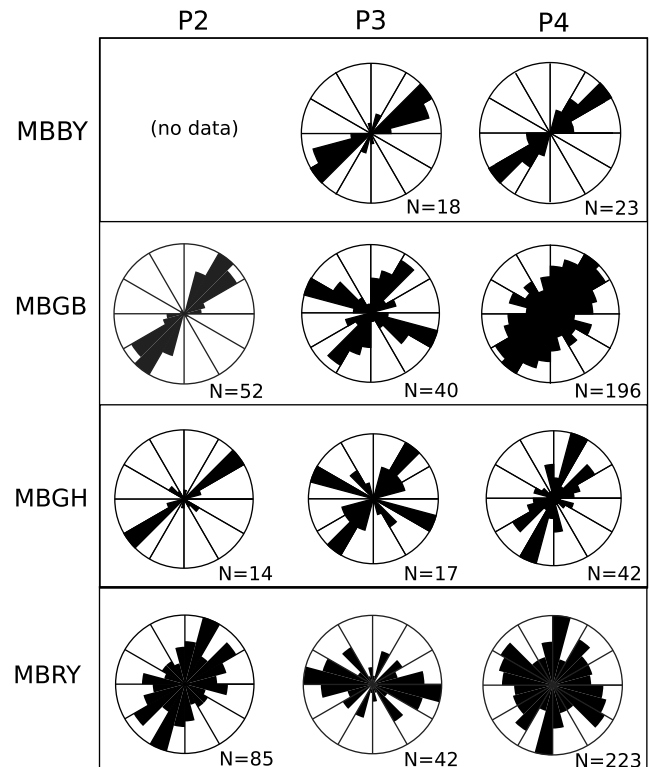

Figure 8. Fitted Von Mises distributions (outer envelopes and heavy black bars) to (a) P axis data and (b) Φ data from period 3. See text for model descriptions.
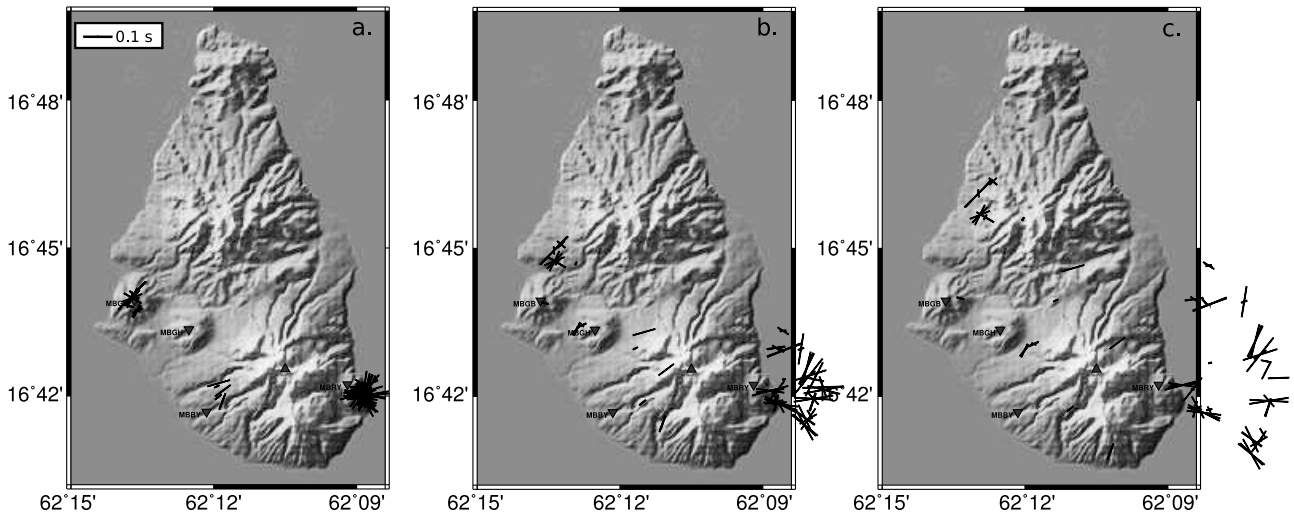

Figure 9. Rose diagrams of A/B quality measurements of Φ (same data as in Figure 6) for individual stations by period for periods 2–4. Only station periods with more than five A/B quality measurements are shown.

Figure 10. Shear wave splitting measurements for period 3 projected to (a) 1 km, (b) 5 km, and (c) 10 km along the raypath from source to receiver. Measurements show fast polarization direction (Φ) as the azimuth of each vector and *dt* as vector length.

inflation model proposed for the FPS data by *Roman et al.* [2008]. To do so, five statistical models are fitted to both the P axis and Φ data: (1) a single axial Von Mises distribution (2 parameters: (μ, κ)), (2) a two-component mixture of axial Von Mises distributions, with common concentration, and means constrained to be 90° apart (3 parameters: (p, μ, κ), where $p_1 = p$ is the mixing fraction of the first component, $p_2 = 1 - p$, $\mu_1 = \mu$, $\mu_2 = \mu + 90°$, $\kappa_1 = \kappa$, and $\kappa_2 = \kappa$), (3) a two-component mixture of axial Von Mises distributions, with equal concentrations, and differing means (4 parameters: $(p, \mu_1, \mu_2, \kappa)$, where $p_1 = p$, $p_2 = 1 - p$, $\kappa_1 = \kappa$, and $\kappa_2 = \kappa$), (4) a two-component mixture of axial Von Mises distributions, with differing concentrations, and means constrained to be 90° apart (4 parameters: $(p, \mu, \kappa_1, \kappa_2)$, where $p_1 = p$, $p_2 = 1 - p$, $\mu_1 = \mu$, $\mu_2 = \mu + 90°$), and (5) a two-component mixture of axial Von Mises distributions, with differing concentrations and means (5 parameters: $(p, \mu_1, \mu_2, \kappa_1, \kappa_2)$, where $p_1 = p$, $p_2 = 1 - p$).
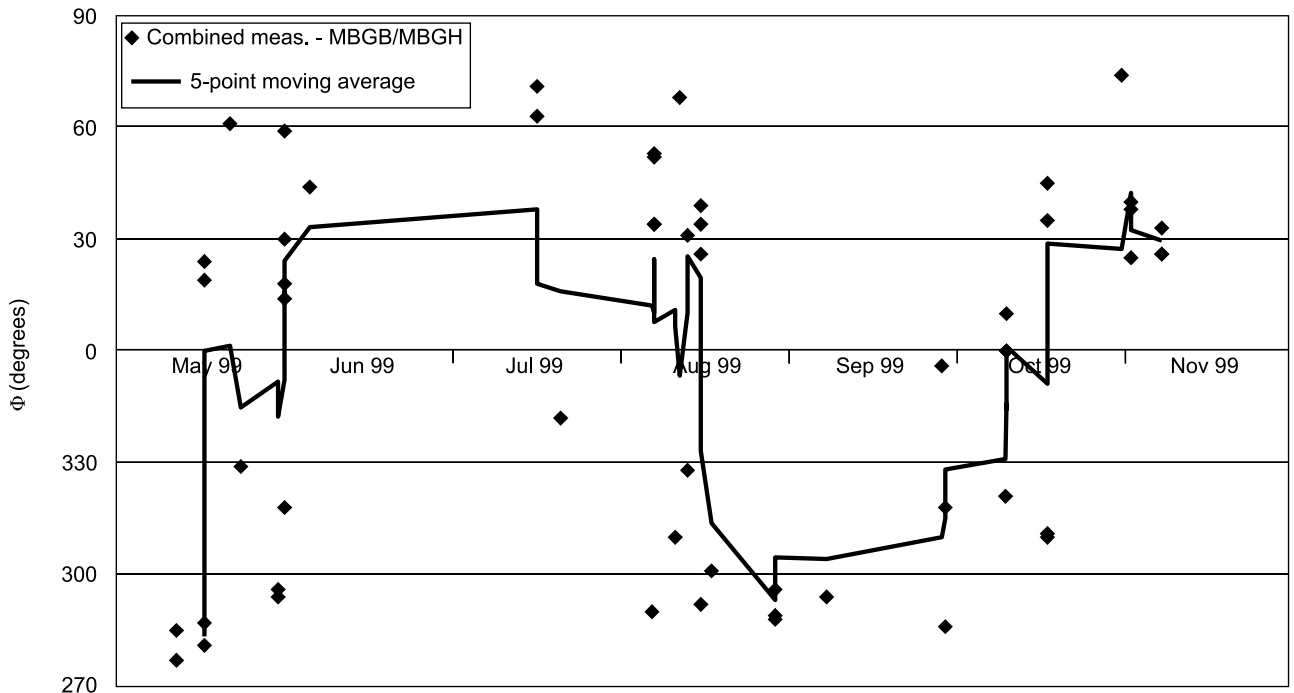
Figure 11. Φ versus time during period 3 on Montserrat stations MBGB and MBGH. Diamonds represent individual measurements, and black line represents a five-point moving average of the individual measurements.

MBGB   MBRY

Period 4
(Excluding
2003)

n=125   n=182

2003 Only

n=71   n=41
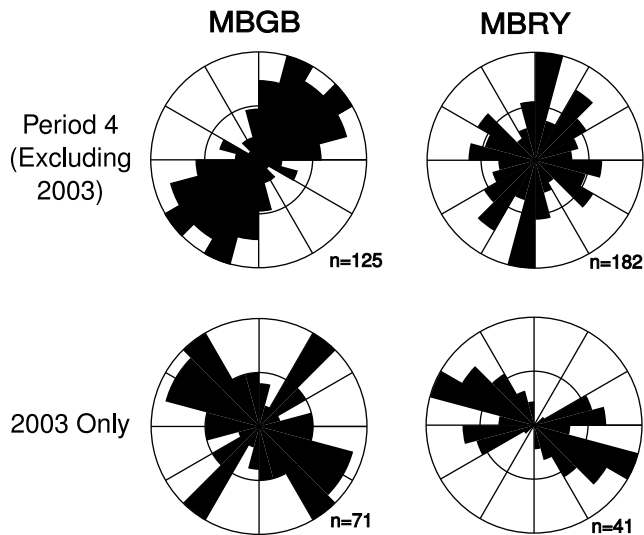
Figure 12. Rose diagrams of Φ on Montserrat stations MBGB and MBRY during subperiods of period 4. (top) Rose diagrams showing period 4 data with measurements from 2003 excluded, and (bottom) rose diagrams showing measurements from 2003 only.

[19] The fitted model parameters are shown in Table 3, and the densities of the fitted models are shown in Figure 8. The preferred model is that with the lowest value of the Akaike Information Criterion (AIC) [*Akaike*, 1974]). Therefore, model 4 (which has differing concentrations but two means constrained to be 90° apart) is preferred for the period 3 P axis data, consistent with the ~90° reorientation of stresses predicted by the dike inflation model. However, model 5 has an AIC value very close to that of model 4, with the orientations of the unconstrained means differing only slightly from the 90° separation in model 4. The preferred

model for the period 3 Φ data is model 3, with clear bimodality and means ~70° (±12°) apart.

4.1.2. Analysis of Individual Station Measurements of Φ

[20] To determine whether spatial variability in the local stress field may explain the apparent nonbimodal heterogeneity in Φ during period 3 (Figure 6), we next examine measurements of Φ on individual Montserrat stations during periods 2–4 (which have the highest number of measurements and encompass the appearance of an ephemeral ~90° "rotated" trend in VT FPS P axis orientation). Individual station measurements of Φ, plotted in Figure 9, indicate that the temporal changes in Φ apparent in rose diagrams of combined measurements (Figure 6b) are also station dependent, indicative of a spatially heterogeneous local stress field. Specifically, during period 3, stations MBGB and MBGH, both located northwest of the Soufrière Hills vent, record the appearance of an ephemeral ~90° rotated trend in Φ with respect to the constant NE-SW oriented trends present at both stations in periods 2, 3, and 4. Station MBRY (east of the vent) records a ~70° change in Φ between periods 2 and 3, and station MBBY (southwest of the vent) does not record a rotation with respect to period 4 (the orientation of Φ in period 2 is poorly constrained for MBBY). The observed rotated trends in Φ on stations MBGB, MBGH, and MBRY during period 3 appear to be independent of event source locations (Figure 10) or initial polarizations. However, while the majority of stations appear to record a single dominant trend in Φ during a given period, stations MBGB and MBGH record a bimodal distribution of Φ in period 3, and stations MBGB and MBRY record heterogeneous Φ orientations during period 4, suggesting additional unresolved temporal stress field variability in periods 3–4 (Figure 9).

[21] During period 3, stations MBGB and MBGH recorded two dominant orientations of Φ, one NE-SW and one
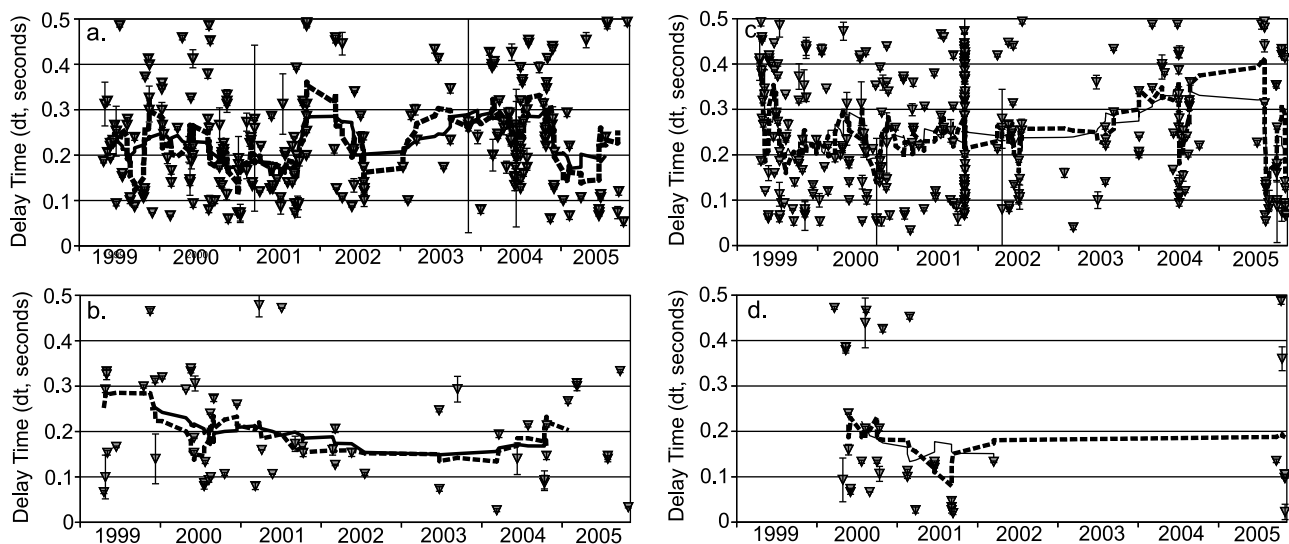
Figure 13. Measurements of *dt* on Montserrat stations (a) MBGB, (b) MBGH, (c) MBRY, and (d) MBBY through time. Triangles show individual measurements, and error bars show 95% confidence intervals for individual measurements. Solid black lines show a 20-point moving average of individual measurements, and dashed black lines show a 10-point moving average of individual measurements.
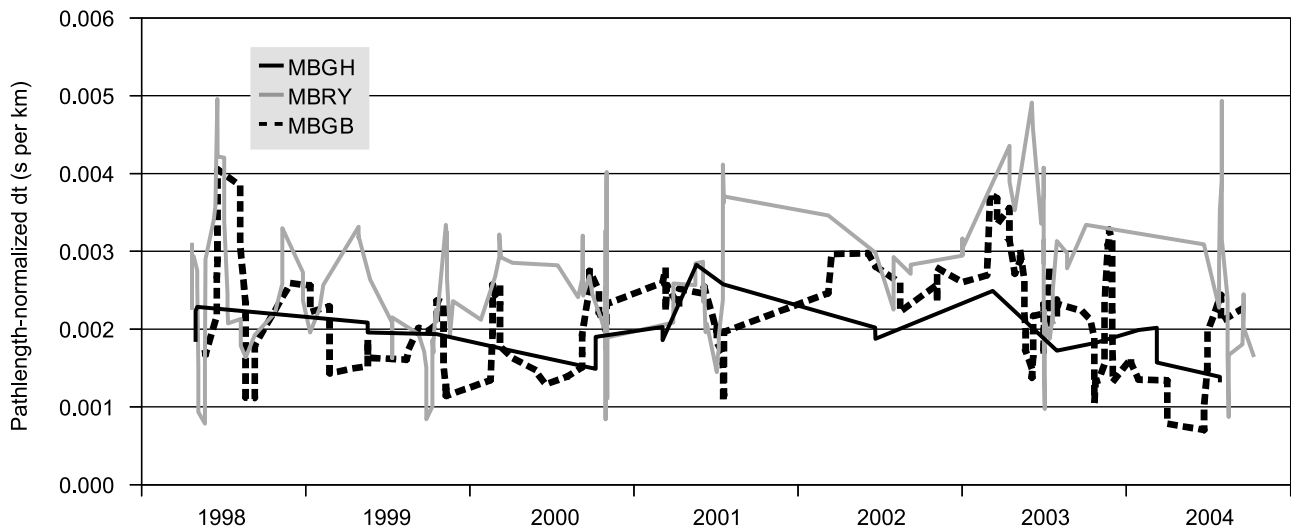
Figure 14. Five-point moving average of measurements of path length-normalized *dt* on Montserrat stations MBGB, MBGH, and MBRY for all events with well-constrained locations during periods 2–4.

NW-SE (Figure 9). As short-term temporal fluctuations in VT FPS orientations were observed during period 3 by *Roman et al.* [2006], we graph individual measurements of Φ from stations MBGB and MBGH versus time in Figure 11 and find a suggestion of an apparent short-term fluctuation in local stress field orientation during this period, consistent with FPS observations. It is likely that these apparent short-term reorientations of local maximum compression, between a background orientation consistent with regional tectonics (NE trending Φ) and a rotated orientation consistent with dike inflation-induced stresses (NW trending Φ), reflect conduit repressurization by "pulses" or "quanta" [e.g., *Scandone*

et al., 2007] of magma as opposed to a continuous and steady influx. Alternatively, the bimodal distributions of Φ may indicate the presence of two fracture sets beneath these stations which respond to both regional stresses and dike injection.

[22] During period 4, stations MBGB and MBRY recorded relatively heterogeneous Φ orientations (Figure 9). We searched for temporal changes in Φ on these two stations and found evidence for a short-term temporal fluctuation in 2003. Figure 12 shows rose diagrams of Φ for MBGB and MBRY in period 4 in which data from 2003 are plotted separately from the remaining data for this
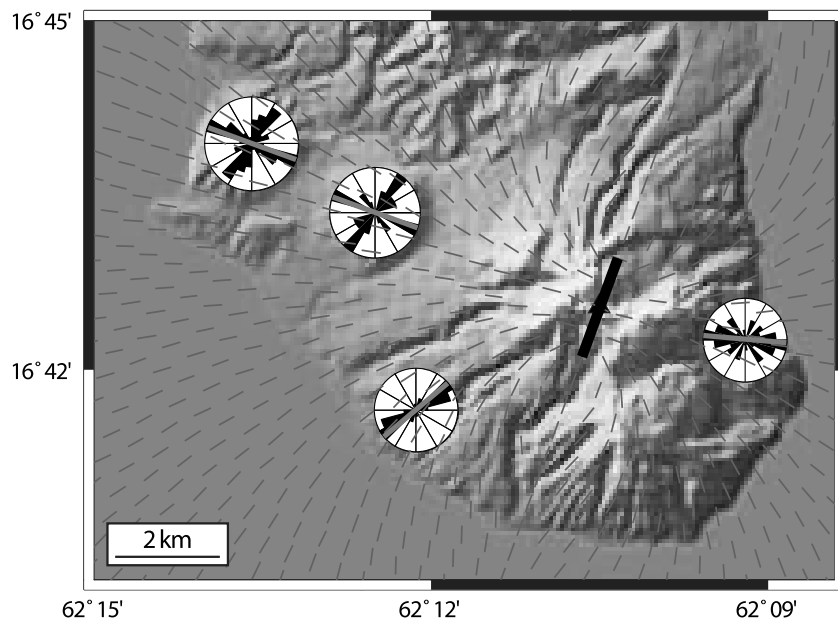
Figure 15. Map of Φ_M orientations (thin gray bars) resulting from 2 m inflation of a 20°-oriented, 2 km long dike (heavy black bar) centered beneath the Soufrière Hills vent. Rose diagrams of Φ for period 3 (Figure 9) are also shown centered on the location of each seismic station (gray bar superimposed on each rose diagram indicates the Φ orientation used for misfit calculation).

**Table 4.** Azimuths of Φ Used for Model Misfit Calculation

Station	Φ Azimuth (deg)
MBBY	50
MBGB	110
MBGH	110
MBRY	95

period. This separation of measurements suggests that a second local stress field reorientation influenced polarizations of split shear waves during 2003: Φ shows a dominant NW-SE orientation on MBGB, and a dominant WNW-ESE orientation on MBRY. Exclusion of the 2003 measurements also significantly reduces the degree of heterogeneity on these two stations during the remainder of period 4. We did not detect changes in Φ on station MBGH during 2003, possibly due to the low number of measurements obtained from this station during period 4 (November 1999 to April 2005). However, we note that for station MBGB, the 2003 orientation of Φ is nearly identical to the period 3 rotated orientation, and for station MBRY the 2003 orientation is again less than ~90° from background Φ as represented by measurements from this station during period 2. The similarity of the change in 2003 to changes observed in period 3 suggests that a similar process caused both changes. Changes in local stress field orientation during 2003 were not apparent in FPS data [e.g., *Roman et al.*, 2006], which suggests that SWS analysis is more sensitive than FPS analysis to subtle degrees of conduit inflation. We note that a major dome collapse event occurred at Soufrière Hills during July 2003 [e.g., *Edmonds and Herd*, 2007], prior to the onset of a 2 year pause in extrusive activity. Our analysis indicates that an increase in pressure in the midlevel to shallow conduit system, consistent with the apparent change in Φ in 2003, may have triggered this dome collapse event. Heterogeneity during this period may also reflect an anisotropic background stress field modulated by weak dike inflation.

[23] Measurements of SWS on Montserrat stations during our study period do not appear to reflect systematic changes in the delay time between split S wavelets (*dt*; Figure 13). Instead, measurements of *dt* appear to be randomly distributed through time, and possibly reflect differences in raypath length and/or crack density along the raypath [e.g., *Hudson*, 1981], rather than changes in the magnitude of inflation-induced stresses through time. Because measurements of *dt* can reflect both raypath length and changes in the magnitude of seismic anisotropy, we plot path length-normalized measurements of *dt* in Figure 14. Normalization of the *dt* measurements reduced their scatter and indicates that measurements of *dt* are similar on all stations. Again, systematic temporal changes in *dt* are not apparent in Figure 14.

4.2. Stress Field Modeling

[24] The ephemeral reorientations of Φ observed during period 3 (and in 2003) range from ~70–90° and precede major changes in the behavior of the Soufrière Hills Volcano; thus, the reorientations are consistent with precursory inflation of a magma-filled dike [e.g., *Gerst and Savage*, 2004; *Roman et al.*, 2006]. Based on this interpretation, we searched for a model of maximum horizontal stress (Φ_M) orientations produced by an inflating dike which maximized agreement between Φ_M trajectories and the distribution of Φ observed on Montserrat during period 3, following the misfit criterion defined in (1). For stations MBGB and MBGH, we assumed that the NW oriented Φ trend (Figure 9), which appears only briefly during the 6 months leading up to the renewal of eruption in November 1999, reflects magma-induced stresses, and that that NE oriented Φ trend, which is constant throughout periods 2–4 (Figure 9), reflects regional stresses. Thus, we use the mode of the NW trends on both stations MBGB and MBGH as Φ for the calculation of model misfit, along with the mode of the single NE trend on MBBY, and the mode of the single WNW-ENE trend on MBRY. We illustrate the azimuths used for Φ in misfit
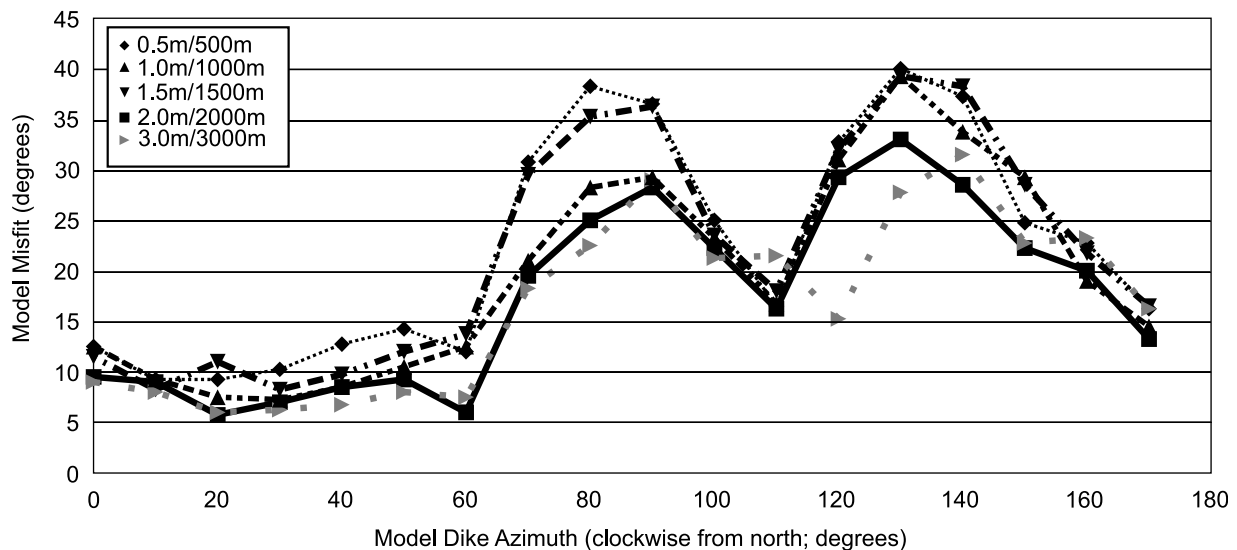
Figure 16. Calculated misfit versus dike azimuth for model dikes of variable widths/lengths (see text for details).

calculations in Figure 15 (gray bars superimposed on rose diagrams) and list them in Table 4. The best fit model (illustrated in Figure 15) is a 2 km long, 2 m wide dike oriented at 20°, subparallel to the regional Φ orientation (Figures 1a and 3a). Inflation of this model dike produces a pattern of induced stresses that is consistent with measurements of Φ observed on all four stations (Figure 15), as indicated a low model misfit of 5.75° for the best fit configuration.

[25] For the 108 models tested, we found a strong dependence of model misfit on dike azimuth, and a weak dependence of model misfit on dike width/length. We graph model misfit versus these two parameters in Figure 16 and show that dike azimuth is well constrained to an orientation of 0–60° (clockwise from north), or approximately NE. Dike width/length is less well constrained, with four out of five tested values producing model misfits below 10° for NE oriented model dikes. The strong agreement between Φ_M vectors and Φ during period 3 indicates that the local stress field reorientation apparent in both SWS and VT earthquake FPS data may be attributed to inflation of a NE trending dike during the 6 months preceding the onset of eruption in November 1999. We attribute the lack of perfect agreement between Φ and Φ_M to a combination of observational error and omission of regional stresses in Φ_M calculations.

5. Discussion

[26] Spatial variations in Φ have been observed on an arc-wide scale in several studies of mantle seismic anisotropy [e.g., *Morley et al.*, 2006; *Nakajima and Hasegawa*, 2004] and have been attributed to a range of mechanisms in the upper mantle wedge, including viscous coupling between plates and convecting mantle [e.g., *Blackman and Kendall*, 2002], and formation of B-type olivine fabrics in regions of high water content and stress [*Jung and Karato*, 2001; *Kneller et al.*, 2005]. Thus, it is important to consider whether the results of our analysis may reflect a component of upper mantle splitting. Although the majority of earthquakes analyzed for this study are located at <40 km depth (Figure 4), we also analyzed waveforms from a small number of earthquakes with depths as great as 180 km BSL, which could hypothetically be affected by anisotropy in the mantle wedge or by lower crustal mineral alignments. While is it difficult to pinpoint the exact depth range of SWS along a raypath, several key features of our results indicate a shallow source of anisotropy and a negligible contribution from mantle processes. First, the observed temporal variation and coincidence of changes in Φ with changes in shallow VT FPS orientations strongly suggests a shallow depth for the splitting layer. It highly unlikely that the temporal variation in Φ reflects changes in the mantle wedge that closely coincided with changes in shallow crustal stress resulting in VT FPS reorientations. Second, measurements of dt are all relatively small (<0.5 s) compared to delay times on the order of 1–2 s reported in studies of splitting attributed to mantle-wedge anisotropy [e.g., *Morley et al.*, 2006; *Nakajima and Hasegawa*, 2004; *Piñero-Feliciangeli and Kendall*, 2008]. Finally, the observed kilometer-scale spatial variations in Φ are difficult to reconcile with large-scale features of mantle flow believed to influence splitting measurements. Therefore, while we cannot rule out some component of

mantle-wedge splitting in our measurements, the main characteristics of our data set are most easily reconciled with an upper crustal source of seismic anisotropy.

[27] Increases in stress large enough to produce the changes apparent in local and regional seismicity at Soufrière Hills may, in theory, also produce detectable surface deformation [e.g., *Savage et al.*, 2010b]. However, published studies of surface deformation observed during the Soufrière Hills eruption have primarily attributed the observed deformation to deep (>5 km) or shallow (<1 km) inflation/deflation sources [e.g., *Foroozan et al.*, 2010, *Mattioli et al.*, 2010, *Elsworth et al.*, 2008; *Wadge et al.*, 2006; *Widiwijayanti et al.*, 2005; *Mattioli and Herd*, 2003; *Mattioli et al.*, 1998]. GPS data from 1997 to 2007 showed radial displacement centered on the vent, which has been interpreted as the result of inflation and deflation of two stacked deep magma chambers located at 6 and 12 km depth based on homogeneous elastic models [*Elsworth et al.*, 2008; *Mattioli and Herd*, 2003] or at 5 and 17 km depth based on heterogeneous elastic models [*Foroozan et al.*, 2010]. In contrast, synthetic aperture radar (SAR) interferograms spanning 1998–2000 and data from a pair of tiltmeters which operated on the flanks of Soufrière Hills from May to August 1997 detect near-field deformation corresponding to shallow (<1 km) pressurization effects within or just below the volcanic edifice and dome [*Wadge et al.*, 2006; *Widiwijayanti et al.*, 2005]. A recent reexamination of the tilt data [*Hautmann et al.*, 2009] found a pattern of displacement consistent with a 163° trending dike.

[28] Two studies published to date have modeled a deformation source in the apparent depth range of the observed stress field changes (i.e., 1–3 km BSL). *Mattioli et al.* [1998] present and analyze episodic GPS measurements from October 1995 to July 1996. These data have been fit with a forward model consisting of an inflating shallow (<3 km) dike trending 140° (only azimuths from 130° to 150° were tested) and a deflating Mogi source located at 6 km [*Mattioli et al.*, 1998]. However, measured ground velocities at several stations have high errors [*Foroozan et al.*, 2010] and the model is poorly constrained: *Mattioli et al.* [2010] and *Foroozan et al.* [2010] reexamined GPS data from 1995 to 2009 and concluded that it was not possible to assess or constrain the geometry of the SHV plumbing system in detail based on GPS data alone. *Linde et al.* [2010] analyze a strain transient recorded by three borehole strainmeters on Montserrat during a sudden Vulcanian explosion on 3 March 2004, and model the explosion source as growth of a 120° trending dike extending from 1.4 to 5 km BSL, coupled with loss of pressure in a deeper Mogi reservoir (stage 1), followed by closure of the dike and a possible accompanying change in the Mogi reservoir (stage 2). They find a close agreement between modeled and observed strains for all three instruments during stage 1 and for the two closest instruments during stage 2.

[29] Reconciliation of our modeling results with the NW oriented model conduits of *Hautmann et al.* [2009] and *Linde et al.* [2010] requires a major transition in conduit orientation and/or geometry (e.g., planar to cylindrical) between the midlevel and shallow level conduit systems at Soufrière Hills [e.g., *Reches and Fink*, 1988], as well as differently oriented but approximately colocated stress and

strain sources which may be activated independently on different timescales or by different volcanic processes (e.g., a sudden explosion versus longer-term pressurization). Alternatively, a more likely explanation is that one of the proposed dike orientations (the approximately NE orientation proposed in this study and by *Roman et al.* [2006, 2008] for the entire eruption period, and by *Miller et al.* [2010] and *Chardot et al.* [2010] for specific subperiods of the eruption; or the NW dike orientation proposed by *Linde et al.* [2010] and *Hautmann et al.* [2009]) is incorrect. We note that we found a local minimum in model misfit consistent with a 3.0/3000 m dike trending 120° (Figure 16), similar to the preferred dike orientation of *Linde et al.* [2010], but that the model misfit for the best fitting NW oriented dike is 15.25°, almost three times higher than the misfit for the best fitting NE oriented model dike. Furthermore, a NW oriented dike is inconsistent with the NE regional Φ orientation (Figure 3a) and the NE orientations of eroded dikes throughout the Lesser Antilles [*Wadge*, 1986]. Similar ~90° ambiguities to that demonstrated in Figure 16 may also exist in models for tilt and strain data. Ultimately, it is likely that some combination of the exclusion of regional stresses and strains from the models; the lack of spatiotemporally dense records of surface deformation, strain, or Φ; the lack of precise knowledge of the current background stress field orientation beneath Montserrat; and poor independent constraints on the exact depth range and dynamics of the conduit system may also contribute to this still unresolved controversy.

[30] The comparative analysis of SWS and FPS presented herein (Figure 6) indicates that local stress field changes indicative of preeruptive conduit pressurization may be detected through careful analysis of local or regional seismic records and used as a basis for midrange forecasts of eruption likelihood. SWS analysis, because it is dependent on moderate to large regional earthquakes, is well suited to background or baseline monitoring during periods of volcanic quiescence, while in contrast FPS analysis provides more detailed temporal resolution of stress field changes during periods of increasing volcano-seismic unrest. As demonstrated herein, data from SWS analysis may also be used to image shallow structures feeding the vent, and may be more sensitive to small increases in stress than VT FPS analysis. As with all monitoring techniques, stress field monitoring has its limitations, the most important demonstrated by this study being the degradation of the trends in and correlation between Φ and FPS P axis orientation beginning in April 2005 (Figure 6). This degradation may ultimately be related to a change in the mechanical nature of the midlevel conduit feeding Soufrière Hills, such as a change in conduit shape (e.g., from planar to cylindrical), an increase in conduit width, or an increase in the density and/or heterogeneity of fractures in the wall rock surrounding the conduit, resulting from 10 years of sustained magma, heat, and volatile flux through this highly active system.

6. Conclusions

[31] We analyzed shear wave splitting in regional earthquake waveforms recorded on seismic stations located on the island of Montserrat between 1996 and 2007 to search for changes in local stress field orientation during the 1995

to present eruption of the Soufrière Hills Volcano. Results of this analysis demonstrate that local stress field reorientations preceding changes in volcanic activity are observable using two independent measures of crustal stress. Changes in split S wavelet polarization (Φ) beneath Montserrat obtained for this study were found to occur contemporaneously with similar (previously documented) reorientations of VT earthquake fault plane solutions for earthquakes located at 1–3 km BSL, indicating an upper crustal source for shear wave splitting. Beginning in May 1999 and persisting until shortly after the onset of eruptive activity in November 1999, the Montserrat stations record azimuthally dependent 0–90° reorientations of Φ. The observed spatial pattern of local changes in Φ during this period is consistent with a model of Φ orientations (Φ_M) resulting from inflation of a NE trending dike. These results conclusively link recently observed preeruptive stress field reorientations beneath Montserrat to dilation of the upper crustal magmatic conduit system and demonstrate that analysis of either regional or local (VT) earthquakes may be used to detect local changes in stress that portend eruptive activity. Furthermore, combined use of SWS analysis and FPS analysis overcomes the limitations of each individual technique for eruption forecasting.

References

Akaike, H. (1974), A new look at the statistical model identification, *IEEE Trans. Autom. Control*, *19*, 716–723, doi:10.1109/TAC.1974.1100705.

Ambeh, W. B., and L. L. Lynch (1996), Seismicity preceding the current eruption of the Soufrière Hills Volcano, Montserrat, West Indies, in *Science, Hazards, and Hazard Management—Volcanism in Montserrat, 2nd Caribbean Conference on Natural Hazards and Disasters*, edited by R. Ahmad, p. 30, Univ. of West Indies, St. Augustine, Trinidad and Tobago.

Beckles, D. M., J. B. Shepherd, and W. P. Aspinall (1977), The Wurst machine: A programme for estimating hypocentral coordinates of regional earthquakes, in *Proceedings of the First Meeting of the Asociacion Ibero-Latino Americana de Geofisica*, edited by E. Gajardo, pp. 95–125, Asoc. Ibero-Latino Am. de Geofis., Caracas, Venezuela.

Beckles, D., J. B. Shepard, and W. P. Aspinall (1992), The "Soufriere" system: PC-based instrumentation for acquiring and processing data from seismograph networks, *Tectonophysics*, *209*, 47–49, doi:10.1016/0040-1951(92)90008-T.

Beroza, G. C., and M. D. Zoback (1993), Mechanism diversity of the Loma Prieta aftershocks and the mechanics of mainshock-aftershock interaction, *Science*, *259*, 210–213, doi:10.1126/science.259.5092.210.

Bianco, F., L. Scarfi, E. Del Pezzo, and D. Patane (2006), Shear-wave splitting time variation associated with the 2001 volcanic eruption of Mt. Etna, *Geophys. J. Int.*, *167*, 959–967, doi:10.1111/j.1365-246X.2006.03152.x.

Blackman, D. K., and J.-M. Kendall (2002), Seismic anisotropy of the upper mantle: 2. Predictions for current plate boundary flow models, *Geochem. Geophys. Geosyst.*, *3*(9), 8602, doi:10.1029/2001GC000247.

Bluth, G. J. S., and W. I. Rose (2004), Observations of eruptive activity at Santiaguito volcano, Guatemala, *J. Volcanol. Geotherm. Res.*, *136*, 297–302, doi:10.1016/j.jvolgeores.2004.06.001.

Bonafede, M., and S. Danesi (1997), Near-field modifications of stress induced by dyke injection at shallow depth, *Geophys. J. Int.*, *130*, 435–448, doi:10.1111/j.1365-246X.1997.tb05659.x.

Bonneton, J. R., and A. E. Scheidegger (1981), Relations between fracture patterns, seismicity and plate motions in the Lesser Antilles, *J. Struct. Geol.*, *3*, 359–369, doi:10.1016/0191-8141(81)90036-5.

Booth, D. C., and S. Crampin (1985), Shear-wave polarizations on a curved wavefront at an isotropic free surface, *Geophys. J. R. Astron. Soc.*, *83*, 31–45.

Bouysse, P., and D. Westercamp (1990), Subduction of Atlantic aseismic ridges and Late Cenozoic evolution of the Lesser Antilles island arc, *Tectonophysics*, *175*, 349–355, doi:10.1016/0040-1951(90)90180-G.

Chardot, L., et al. (2010), Explosion dynamics from strainmeter and microbarometer observations, Soufrière Hills Volcano, Montserrat: 2008–2009, *Geophys. Res. Lett.*, *37*, L00E24, doi:10.1029/2010GL044661.

Cortés, G. P., and A. J. Raigosa (1997), A synthesis of the recent activity of Galeras volcano, Colombia: Seven years of continuous surveillance, 1989–1995, *J. Volcanol. Geotherm. Res.*, *77*, 101–114, doi:10.1016/S0377-0273(96)00089-3.

DeMets, C., P. E. Jansma, G. S. Mattioli, T. H. Dixon, F. Farina, R. Bilham, E. Calais, and P. Mann (2000), GPS geodetic constraints on Caribbean–North American plate motion, *Geophys. Res. Lett.*, *27*, 437–440, doi:10.1029/1999GL005436.

Edmonds, M., and R. A. Herd (2007), A volcanic degassing event at the explosive-effusive transition, *Geophys. Res. Lett.*, *34*, L21310, doi:10.1029/2007GL031379.

Elsworth, D., G. Mattioli, J. Taron, B. Voight, and R. Herd (2008), Implications of magma transfer between multiple reservoirs on eruption cycling, *Science*, *322*, 246–248, doi:10.1126/science.1161297.

Foroozan, R., D. Elsworth, B. Voight, and G. S. Mattioli (2010), Dual reservoir structure at Soufrière Hills Volcano inferred from continuous GPS observations and heterogeneous elastic modeling, *Geophys. Res. Lett.*, *37*, L00E12, doi:10.1029/2010GL042511.

Garcia-Aristizabal, A., H. Kumagai, P. Samaniego, P. Mothes, H. Yepes, and M. Monzier (2007), Seismic, petrologic, and geodetic analysis of the 1999 dome-forming eruption of Guagua Pichincha volcano, Ecuador, *J. Volcanol. Geotherm. Res.*, *161*, 333–351, doi:10.1016/j.jvolgeores.2006.12.007.

Gardner, C. A., and R. A. White (2002), Seismicity, gas emission and deformation from 18 July to 25 September 1995 during the initial phreatic phase of the eruption of Soufrière Hills Volcano, Montserrat, in *The Eruption of Soufrière Hills Volcano, Montserrat, From 1995 to 1999*, edited by T. H. Druitt and B. P. Kokelaar, *Geol. Soc. Mem.*, *21*, 567–582.

Gerst, A., and M. K. Savage (2004), Seismic anisotropy beneath Ruapehu Volcano: A possible eruption forecasting tool, *Science*, *306*, 1543–1547, doi:10.1126/science.1103445.

Harford, C. L., M. S. Pringle, R. S. J. Sparks, and S. R. Young (2002), The volcanic evolution of Montserrat using $^{40}Ar/^{39}Ar$ geochronology, in *The Eruption of Soufrière Hills Volcano, Montserrat, From 1995 to 1999*, edited by T. H. Druitt and B. P. Kokelaar, *Geol. Soc. Mem.*, *21*, 93–114.

Hautmann, S., J. Gottsmann, S. Sparks, A. Costa, O. Melnik, and B. Voight (2009), Modelling ground deformation caused by oscillating overpressure in a dyke conduit at Soufrière Hills Volcano, Montserrat, *Tectonophysics*, *471*, 87–95, doi:10.1016/j.tecto.2008.10.021.

Hudson, J. A. (1981), Wave speeds and attenuation of elastic waves in material containing cracks, *Geophys. J. R. Astron. Soc.*, *64*, 133–150.

Jung, H., and S. Karato (2001), Water-transitions in olivine, *Science*, *293*, 1460–1463, doi:10.1126/science.1062235.

Kneller, E., P. E. van Keren, S. Karato, and J. Park (2005), B-type olivine fabric in the mantle wedge: Insights from high-resolution non-Newtonian subduction zone models, *Earth Planet. Sci. Lett.*, *237*, 781–797, doi:10.1016/j.epsl.2005.06.049.

Kokelaar, B. P. (2002), Setting, chronology, and consequences of the eruption of Soufrière Hills Volcano, Montserrat (1995–1999), in *The Eruption of Soufrière Hills Volcano, Montserrat, From 1995 to 1999*, edited by T. H. Druitt and B. P. Kokelaar, *Geol. Soc. Mem.*, *21*, 1–44.

Lehto, H. L., D. C. Roman, and S. C. Moran (2010), Temporal changes in stress preceding the 2004–2008 eruption of Mount St. Helens, Washington, *J. Volcanol. Geotherm. Res.*, *198*, 129–142, doi:10.1016/j.jvolgeores.2010.08.015.

Lin, J., and R. S. Stein (2004), Stress triggering in thrust and subduction earthquakes and stress interaction between the southern San Andreas and nearby thrust and strike-slip faults, *J. Geophys. Res.*, *109*, B02303, doi:10.1029/2003JB002607.

Linde, A. T., et al. (2010), Vulcanian explosion at Soufrière Hills Volcano, Montserrat on March 2004 as revealed by strain data, *Geophys. Res. Lett.*, *37*, L00E07, doi:10.1029/2009GL041988.

Lipman, P. W., and D. R. Mullineaux (1981), The 1980 eruptions of Mount St. Helens, Washington, *U.S. Geol. Surv. Prof. Pap.*, *1250*.

Luckett, R., B. Baptie, and L. Ottemoller (2007), Seismic monitoring of the Soufrière Hills Volcano, Montserrat, *Seismol. Res. Lett.*, *78*, 192–200, doi:10.1785/gssrl.78.2.192.

Mardia, K. V., and P. E. Jupp (2000), *Directional Statistics*, John Wiley, Chichester, U. K.

Mattioli, G. S., and R. Herd (2003), Correlation of cyclic surface deformation recorded by GPS geodesy with surface magma flux at Soufrière Hills Volcano, Montserrat, *Seismol. Res. Lett.*, *74*, 230.

Mattioli, G. S., T. H. Dixon, F. Farina, E. S. Howell, P. E. Jansma, and A. L. Smith (1998), GPS measurement of surface deformation around Soufrière Hills Volcano, Montserrat from October 1995 to July 1996, *Geophys. Res. Lett.*, *25*, 3417–3420, doi:10.1029/98GL00931.

Mattioli, G. S., R. A. Herd, M. H. Strutt, G. Ryan, C. Widiwijayanti, and B. Voight (2010), Long term surface deformation of Soufrière Hills Volcano, Montserrat from GPS geodesy: Inferences from simple elastic inverse models, *Geophys. Res. Lett.*, *37*, L00E13, doi:10.1029/2009GL042268.

McCann, W. R., and W. D. Pennington (1990), Seismicity, large earthquakes, and the margin of the Caribbean Plate, in *The Geology of North America*, vol. H, *The Caribbean Region*, edited by G. Dengo and J. E. Case, pp. 291–306, Geol. Soc. of Am., Boulder, Colo.

Miller, A. D., R. C. Stewart, R. A. White, R. Luckett, B. J. Baptie, W. P. Aspinall, J. L. Latchman, L. L. Lynch, and B. Voight (1998), Seismicity associated with dome growth and collapse at the Soufrière Hills Volcano, Montserrat, *Geophys. Res. Lett.*, *25*, 3401–3404, doi:10.1029/98GL01778.

Miller, V., B. Voight, C. J. Ammon, E. Shalev, and G. Thompson (2010), Seismic expression of magma-induced crustal strains and localized fluid pressures during initial eruptive stages, Soufriere Hills Volcano, Montserrat, *Geophys. Res. Lett.*, *37*, L00E21, doi:10.1029/2010GL043997.

Morley, A. M., G. W. Stuart, J.-M. Kendall, and M. Reyners (2006), Mantle wedge anisotropy in the Hikurangi subduction zone, central North Island, New Zealand, *Geophys. Res. Lett.*, *33*, L05301, doi:10.1029/2005GL024569.

Murphy, M. D., R. S. J. Sparks, J. Barclay, M. J. Carroll, and T. S. Brewer (2000), Remobilisation of andesite magma by intrusion of mafic magma at the Soufrière Hills volcano, Montserrat, West Indies, *J. Petrol.*, *41*, 21–42, doi:10.1093/petrology/41.1.21.

Nakada, S., H. Shimizu, and K. Ohta (1999), Overview of the 1990–1995 eruption at Unzen Volcano, *J. Volcanol. Geotherm. Res.*, *89*, 1–22, doi:10.1016/S0377-0273(98)00118-8.

Nakajima, J., and A. Hasegawa (2004), Shear-wave polarization anisotropy and subduction-induced flow in the mantle wedge of northeastern Japan, *Earth Planet. Sci. Lett.*, *225*, 365–377, doi:10.1016/j.epsl.2004.06.011.

Okada, Y. (1992), Internal deformation due to shear and tensile faults in a half-space, *Bull. Seismol. Soc. Am.*, *82*, 1018–1040.

Paulatto, M., et al. (2010), Upper crustal structure of an active volcano from refraction/reflection tomography, Montserrat, Lesser Antilles, *Geophys. J. Int.*, *180*, 685–696, doi:10.1111/j.1365-246X.2009.04445.x.

Piñero-Feliciangeli, L. T., and J.-M. Kendall (2008), Sub-slab mantle flow parallel to the Caribbean plate boundaries: Inferences from SKS splitting, *Tectonophysics*, *462*, 22–34, doi:10.1016/j.tecto.2008.01.022.

Reches, Z., and J. Fink (1988), The Mechanism of Intrusion of the Inyo Dike, Long Valley Caldera, California, *J. Geophys. Res.*, *93*(B5), 4321–4334, doi:10.1029/JB093iB05p04321.

Roman, D. C. (2005), Numerical models of volcanotectonic earthquake triggering on non-ideally oriented faults, *Geophys. Res. Lett.*, *32*, L02304, doi:10.1029/2004GL021549.

Roman, D. C., S. C. Moran, J. A. Power, and K. V. Cashman (2004), Temporal and spatial variation of local stress fields during the 1992 eruptions of Crater Peak vent, Mount Spurr Volcano, Alaska, *Bull. Seismol. Soc. Am.*, *94*, 2366–2379, doi:10.1785/0120030259.

Roman, D. C., J. Neuberg, and R. R. Luckett (2006), Assessing the likelihood of volcanic eruption through analysis of volcanotectonic earthquake fault-plane solutions, *Earth Planet. Sci. Lett.*, *248*, 229–237, doi:10.1016/j.epsl.2006.05.029.

Roman, D. C., S. De Angelis, J. Latchman, and R. A. White (2008), Patterns of volcanotectonic seismicity and stress during the ongoing eruption of the Soufrière Hills Volcano, Montserrat (1995–2007), *J. Volcanol. Geotherm. Res.*, *173*, 230–244, doi:10.1016/j.jvolgeores.2008.01.014.

Savage, M. K., X. R. Shih, R. P. Meyer, and R. C. Aster (1989), Shear-wave anisotropy of active tectonic regions via automated S-wave polarization analysis, *Tectonophysics*, *165*, 279–292, doi:10.1016/0040-1951(89)90053-X.

Savage, M. K., A. Wessel, N. A. Teanby, and A. W. Hurst (2010a), Automatic measurement of shear wave splitting and applications to time varying anisotropy at Mount Ruapehu volcano, New Zealand, *J. Geophys. Res.*, *115*, B12321, doi:10.1029/2010JB007722.

Savage, M. K., T. Ohminato, Y. Aoki, H. Tsuji, and S. Greve (2010b), Absolute stress and its temporal variation at Mt. Asama Volcano, Japan, from seismic anisotropy and GPS, *Earth Planet. Sci. Lett.*, *290*, 403–414, doi:10.1016/j.epsl.2009.12.037.

Scandone, R., K. V. Cashman, and S. D. Malone (2007), Magma supply, magma ascent and the style of volcanic eruptions, *Earth Planet. Sci. Lett.*, *253*, 513–529, doi:10.1016/j.epsl.2006.11.016.

Sherrod, D. R., W. E. Scott, and P. H. Stauffer (2008), A volcano rekindled; the renewed eruption of Mount St. Helens, 2004–2006, *U.S. Geol. Surv. Prof. Pap.*, *1750*.

Silver, P. G., and W. W. Chan (1991), Shear wave splitting and subcontinental mantle deformation, *J. Geophys. Res.*, *96*, 16,429–16,454, doi:10.1029/91JB00899.

Stein, S., J. Engeln, D. Wiens, K. Fujita, and R. Speed (1982), Subduction seismicity and tectonics in the Lesser Antilles Arc, *J. Geophys. Res.*, *87*, 8642–8664, doi:10.1029/JB087iB10p08642.

Stein, S., C. DeMets, R. G. Gordon, J. Brodholt, D. Argus, J. F. Engeln, P. Lundgren, C. Stein, D. A. Wiens, and D. F. Woods (1988), A test of alternative Caribbean Plate relative motions, *J. Geophys. Res.*, *93*, 3041–3050, doi:10.1029/JB093iB04p03041.

Tadokoro, K., and M. Ando (2002), Evidence for rapid fault healing derived from temporal changes in S wave splitting, *Geophys. Res. Lett.*, *29*(4), 1047, doi:10.1029/2001GL013644.

Teanby, N., J.-M. Kendall, and M. van der Baan (2004), Automation of shear-wave splitting measurements using cluster analysis, *Bull. Seismol. Soc. Am.*, *94*, 453–463, doi:10.1785/0120030123.

Toda, S., R. S. Stein, K. Richards-Dinger, and S. B. Bozkurt (2005), Forecasting the evolution of seismicity in southern California: Animations built on earthquake stress transfer, *J. Geophys. Res.*, *110*, B05S16, doi:10.1029/2004JB003415.

Umakoshi, K., H. Shimizu, and N. Matsuwo (2001), Volcano-tectonic seismicity at Unzen Volcano, Japan, 1985–1999, *J. Volcanol. Geotherm. Res.*, *112*, 117–131, doi:10.1016/S0377-0273(01)00238-4.

Wadge, G. (1986), The dykes and structural setting of the volcanic front in the Lesser Antilles island arc, *Bull. Volcanol.*, *48*, 349–372, doi:10.1007/BF01074466.

Wadge, G., G. S. Mattioli, and R. A. Herd (2006), Ground deformation at Soufrière Hills Volcano, Montserrat during 1998–2000 measured by radar interferometry and GPS, *J. Volcanol. Geotherm. Res.*, *152*, 157–173, doi:10.1016/j.jvolgeores.2005.11.007.

Watson, G. S., and E. J. Williams (1956), On the construction of significance tests on the circle and the sphere, *Biometrika*, *43*, 344–352.

Wessel, A. (2008), Automatic shear wave splitting measurements at Mt. Ruapehu volcano, New Zealand, M.Sc. thesis, Sch. of Earth and Environ., Victoria Univ. of Wellington, Wellington, New Zealand.

Widiwijayanti, C., A. Clarke, D. Elsworth, and B. Voight (2005), Geodetic constraints on the shallow magma system at Soufrière Hills Volcano, Montserrat, *Geophys. Res. Lett.*, *32*, L11309, doi:10.1029/2005GL022846.

Zatsepin, S. V., and S. Crampin (1997), Modelling the compliance of crustal rock—I. Response of shear-wave splitting to differential stress, *Geophys. J. Int.*, *129*, 477–494, doi:10.1111/j.1365-246X.1997.tb04488.x.

R. Arnold, School of Mathematics, Statistics, and Operations Research, Victoria University of Wellington, PO Box 600, Wellington 6140, New Zealand.

S. De Angelis, Montserrat Volcano Observatory, British Geological Survey, Flemings, Montserrat.

J. L. Latchman, Seismic Research Centre, University of the West Indies, St. Augustine, Trinidad and Tobago.

D. C. Roman, Department of Geology, University of South Florida, 4202 E. Fowler Ave., SCA 528, Tampa, FL 33620, USA. (droman@usf.edu)

M. K. Savage, School of Geography, Environment and Earth Sciences, Victoria University of Wellington, PO Box 600, Wellington 6140, New Zealand.